Chemical Engineering Journal 146 (2009) 503–514

Contents lists available at ScienceDirect

Chemical Engineering Journal

journal homepage: www.elsevier.com/locate/cej

Tuning interfacial non-covalent interactions through biomimetic functionalization of inorganic surface: The case of lysozyme and mesocellular silica foam hybrids

Shan Lu, Jing He*, Zhijun Liu

State Key Laboratory of Chemical Resource Engineering, Beijing University of Chemical Technology, Box 98, Beijing 100029, China

ARTICLE INFO

Article history:
Received 9 July 2008
Received in revised form 15 October 2008
Accepted 23 October 2008

Keywords:
Protein adsorption
Mesocellular silica foam
Biomimetic modification
Non-covalent interactions
Bio-inorganic hybrids

ABSTRACT

The mesocellular silica foam (MCF) surface has been functionalized with –OH, $-C_3H_6H$, $-C_3H_6NH_2$, $-C_3H_6NHCONH_2$, and $-C_3H_6COOH$ biomimetic groups. Thereby the non-covalent interaction between protein and support surface is generated and tailored in virtue of the surface modification and varied pH of adsorption medium. The adsorption kinetics, adsorption thermodynamics, protein distribution and adsorption reversibility have been discussed in relation to the surface–protein interfacial interactions and protein–protein lateral interactions. It is found that between lysozyme and MCF surfaces, the electrostatic force, hydrophobic interaction, π–π overlapping, and some hydrogen bonding are similarly effective driving forces for protein adsorption. But depending on the nature of interfacial interactions, the effects of protein–protein repulsion on the lysozyme adsorption are diversified. The biomimetic modification of inorganic support surface counteracts in part the inhibition effects of protein–protein repulsion on protein adsorption, thus favoring the adsorption capacity. The adsorption of lysozyme on MCF supports causes no visible loss of enzymatic activity.

1. Introduction

Mesoporous silicas, discovered in early 1990s and developed vigorously since then [1–7], offer the possibility of entrapping large biomolecules within their nano-sized pores [8–10]. Mesoporous materials not only have highly ordered pore structures with uniform pore diameters and large surface areas, but they also are liable to chemical modification and functionalization. These properties, combined with good chemical stability, make them competent candidates for designed biocatalysts, protein-separation devices, drug delivery systems, and biosensors. Considering the different applications, the protein adsorption heterogeneities including adsorption capacity, permanent or reversible feature, and protein distribution on the mesoporous host are needed. For example, rapid permanent monolayer adsorption is preferred for a biocatalyst, while as little as possible irreversible adsorption of proteins on chromatographic supports is required for bio-separation. Thus, understanding the features of protein adsorption in mesoporous silica is of great interest and significance.

The major factors that might influence protein adsorption in mesoporous hosts involve the spatial factors and interfacial interactions. Morphologies (spheres, films, monoliths, rod-like or fibrous agglomerates) and particle sizes usually make impact on adsorption as spatial factor [8,11–17]. In addition, three-dimensional structures always have more accessible pores for proteins than one-dimensional structures [18]. Generally, a certain pore size, neither too small to exclude large proteins nor too large to drain proteins easily, can reach the highest adsorption capacity [19]. The interfacial interactions between proteins and support surfaces are more complex than spatial factors. Interfacial interactions between proteins and mesoporous silica mainly contain covalent and non-covalent interactions. Usually, the host–guest covalent interactions which result from fierce interfacial chemical reactions and format a new molecule lead to irreversible adsorption of proteins [20]. The non-covalent interactions extensively existing in the bio-macromolecules such as DNA and proteins, which lead to the formation of the host–guest or guest–guest clusters, are supposed to play an important role in protein adsorption. The typical non-covalent forces include hydrogen bonding, electrostatic forces, hydrophobic interactions, and some specific non-covalent interactions [21]. So the charge feature and hydrophobicity of support surface, isoelectric point and surface property of protein, as well as pH and ion strength of adsorption solution might all independently or dependently influence the interfacial non-covalent interactions [22,23]. Several publications reported the effects of electrostatic interactions on protein adsorption [13,15,24–27], while some

* Corresponding author. Tel.: +86 10 64425280; fax: +86 10 64425385.
E-mail addresses: jinghe@263.net.cn, hejing@mail.buct.edu.cn (J. He).

1385-8947/$ – see front matter © 2008 Elsevier B.V. All rights reserved.
doi:10.1016/j.cej.2008.10.032

others involved the roles of hydrophobicity, hydrogen bonding, and protein–protein lateral interactions [28–31]. The adsorption behaviors of proteins, together with other organic molecules, on silica surface have been reviewed recently by Parida et al. [32].

Mesocellular siliceous foam (MCF) with mesocellular pores connected by mesoporous windows is chosen as host for lysozyme in this work. The ultra-large pore size and three-dimensional interconnected pore structure of MCF are supposed to cause less spatial restriction to proteins than one-dimensional channels of MCM-41 and SBA-15. So it should be more appropriate to survey interfacial interactions in protein–MCF hybrid systems. Only few publications about protein adsorption on MCF have been reported till now, however [11,33,34]. Han et al. demonstrated MCF could serve as combined size-exclusion and ion-exchange supports [11], and used MCF to immobilize chloroperoxidase for the first time [33]. Recently, CALB was successfully entrapped in hydrophobic MCF by pressure-driven method, displaying excellent catalytic performance [34].

The interfacial non-covalent interactions in lysozyme-MCF hybrids are generated and tailored in this work through modifying MCF surface with –OH, $-C_3H_6H$, $-C_3H_6NH_2$, $-C_3H_6NHCONH_2$, and $-C_3H_6COOH$ groups and varying the pH of adsorption medium. The electrostatic interactions could be derived from the unprotonated terminal –Si–OH, –COOH, protonated terminal $-NH_2$ or $-NHCONH_2$ on solid surface with charged protein. Hydrophobic interactions are from terminal alkyls on solid surface and side chains of amino acid residues in protein. Hydrogen bonding interaction occurs between –Si–OH, –COOH, $-NH_2$ on support surface and $-NH_2$ or –COOH in protein. The π–π overlapping interactions could be expected between surface $-NHCONH_2$ and the surfacial peptide bonds in protein.

Lysozyme (EC 3.2.1.17), present in such places as chicken egg white, human tears, fish serum and insect saliva, is an enzyme that attacks bacterial cell walls. It could catalyze the hydrolysis of glycosidic bonds of muramic acids in mureins, and is also capable of degrading chitin. So lysozyme is widely used in medicine and food industry for its high antifunga, antibacterial and antiviral efficiency [35]. Lysozyme, with its structure well determined, is a prolate spheroid protein with two characteristic cross-sections of 3.0 nm × 4.5 nm and 3.0 nm × 3.0 nm, a molecular weight of 14.4 kDa, and a pI of 11 [24]. Lysozyme is stable between pH 1.5 and 12, which grants lysozyme a fine model protein for interfacial adsorption in a wide range of pH.

2. Experimental

2.1. Materials

Pluronic P123 (Mav = 5800, Aldrich), 1,3,5-trimethylbenzene (TMB) (98%, Fluka), n-propyltriethoxysilane (PTOS) (98%, Jingzhou Jianghan Fine Chemical Co., Ltd.), 3-aminopropyltriethoxysilane (APTS) (98.5%, Jingzhou Jianghan Fine Chemical Co., Ltd.), 3-ureidopropyltriethoxysilane (UPTS) (50% in methanol, Jingzhou Jianghan Fine Chemical Co., Ltd.), 4-(triethoxysilyl)butyronitrile (TSBN) (98%, Aldrich), tetraethoxysilane (TEOS) (Beijing Chemical Factory), toluene (Beijing Chemical Factory), and benzophenone (Beijing Chemical Factory) are all of analytical-grade purity and used as received (if no further statement). Hen egg white lysozyme (2 × crystallized, lyophilized, 20,000 units/mg of protein) is from Sinopharm Chemical Reagent Co., Ltd. (stored at 0–4 °C) and *Micrococcus lysodeikticus* dried cells from Sigma.

2.2. Preparation and modification of MCF

MCF was synthesized following the reported procedure [34] with some modifications. 4 g of P123 was dissolved in the mixture solution of 65 mL of deionized water and 10 mL of 12 M aqueous HCl. 2.96 g of TMB was added. The solution was stirred vigorously at 40 °C for 2 h. 8.95 g of TEOS was slowly introduced, followed by aging at 40 °C for 20 h. 46.0 mg of NH_4F in 5 mL of deionized water was then added, agitated for another 30 s. The agitation here is important for the formation of pores with a uniform narrow rather than a bimodal distribution. The mixture was then kept at 100 °C in a Teflon autoclave for 48 h. The white solid was filtered, washed with deionized water and ethanol, dried at ambient temperature. After calcination at 550 °C for 6 h to remove P123, MCF was activated in the following procedure [36]: (1) immerse 3.0 g of MCF into a mixture solution of aqueous HCl and MeOH (1:1, V/V) (40 mL) at room temperature for 30 min. Rinse the silica three times with deionized water. (2) Immerse the silica into 25 mL of concentrated H_2SO_4 (98%) at room temperature for 30 min. Rinse the silica well with deionized water. It is important to remove all H_2SO_4 residues from the solid in order to make a uniform silane monolayer. (3) Boil the silica for 30 min in 150 mL of deionized water. The resulting solid was filtered, dried at room temperature for 12 h and then at 100 °C for 2 h, to give activated MCF, denoted MCF–OH. Triethoxysilanes $(EtO)_3Si–X$ (X = C_3H_6H, $C_3H_6NH_2$, $C_3H_6NHCONH_2$ and C_3H_6CN) were used to generate different silica surfaces. Typically [37], 1.0 g of MCF–OH, which was pre-treated in 150 °C oven for 2 h before its usage, was suspended in 40 mL of toluene (99.7%, dehydrated by refluxing the mixture of 500 mL toluene, 1 g Na, and 5 mg benzophenone as visual indicator for approximately 5 h). Then 5 mmol of triethoxysilane (calculated from the maximum grafting amount based on assumption of 5×10^{18} molecules/m^2 in fully dense monolayer coverage) was added. The mixture was refluxed at 108 °C for 24 h. The white solid was filtered, washed with diethyl ether, and dried in air. The samples were denoted MCF–X, where X is the functional group on the surface. MCF–C_3H_6COOH was produced by refluxing MCF–C_3H_6CN in aqueous HCl (35.5 wt.%) for 24 h.

2.3. Characterization

Nitrogen sorption isotherms were measured at 77 K using a Quantachrome Autosorb-1 system. The pore size distribution was calculated using the BJH (Barrett–Joyner–Halenda) method. The specific surface area was calculated using the Brunauer–Emmett–Teller (BET) method based on the adsorption branch. FT-IR spectra were recorded on a Bruker Vector 22 spectrometer at 1 cm^{-1} resolution, the samples being pressed into disks with KBr. The FT-IR spectra in the amide I region (1600–1700 cm^{-1}) were analyzed using Lorentz curve-fitting (by Origin 7.0) method. The frequencies of the band centers found in the spectra were used as stating parameters and a value of 16 for roughly validating the width of peaks. In most instances, the discrepancies between the component frequencies obtained from the spectral and curve fitting were below 3 cm^{-1}. All component peaks were assigned to the specific secondary structure components according to references [38,39]. The band at 1633 ± 2 cm^{-1} was assigned to β-sheet, 1656 ± 2 cm^{-1} to α-helix, 1668 ± 2 cm^{-1} to β-turns, 1622 ± 2 cm^{-1}, 1644 ± 2 cm^{-1}, and 1682 ± 2 cm^{-1} to random coils and others. The secondary structure contents were calculated from the areas of the individual assigned bands and their fraction of total area in the amide I region. Scanning electron micrographs (SEM) were taken on a Cambridge S-250MK3 microscope. Transmission electron micrographs (TEM) were taken on a FEI Tecnai 20 electron microscope operating at 200 kV. CHN element analysis was carried out on an Elementar Vario EL III elemental analyzer. The UV absorption data were collected on a Shimadzu UV-2501 spectrometer.

2.4. Lysozyme adsorption and desorption

25 mM buffer solutions with different pH were first prepared, citric acid–dibasic sodium phosphate buffer for pH 4.8, potassium dihydrogen phosphate–dibasic sodium phosphate buffer for pH 6.8, and sodium carbonate–sodium bicarbonate buffer for pH 10.0 and 12.0. A series of standard lysozyme solutions with the concentration ranging from 0.2 to 6.0 mg/mL were prepared by dissolving different amounts of lysozyme in the above-mentioned buffer solutions. In the adsorption experiment dealing with adsorption capacity and kinetics, 15 mg of the MCF–X (X = OH, C_3H_6H, $C_3H_6NH_2$, $C_3H_6NHCONH_2$, and C_3H_6COOH) adsorbent was immerged in 10 mL of 1 mg/mL lysozyme solution and was oscillated at 298 K for 180 h with a speed of 130 r/min. The mixture was sampled at different intervals and centrifuged at 5000 r/min for 10 min to monitor the lysozyme concentration in supernatant. Then the supernatant liquid was re-mixed with the adsorbent by vortex. The adsorbed amount of lysozyme on MCFs was calculated by subtracting the lysozyme in supernatant from the total lysozyme amount. The lysozyme amount was determined by the UV absorption at 280 nm. The resulting MCF materials with lysozyme adsorbed are denoted MCF–X–Lz (X = OH, C_3H_6H, $C_3H_6NH_2$, $C_3H_6NHCONH_2$, and C_3H_6COOH). In the pseudo-isotherm experiments for protein distribution, 15 mg of the MCF–X adsorbent was immerged in 5 mL of 0.2–6.0 mg/mL lysozyme solution, respectively, and was oscillated for 24 h. In the desorption experiments, 15 mg of the MCF–X adsorbent was first immerged in 5 mL of 0.6 mg/mL lysozyme solutions for 24 h at pH 6.8 and 10, respectively. After measuring the adsorption amount, the washed adsorbent was immerged in blank buffers at the same pH as in the adsorption solution for 24 h to measure the percentage leaching of lysozyme.

2.5. Activity assay

9 mg of *M. lysodeikticus* cell was added in 30 mL of 0.1 M, pH 6.2 phosphate buffers and stirred slowly for 10 min at room temperature to prepare the cell suspension. The cell suspension should be used in 1 h later than preparation. 5 mg of native lysozyme was dissolved in 100 mL of pH 6.2 phosphate buffers to obtained 50 μg/mL enzyme solution. At room temperature (25 °C), 100 μL of enzyme solution was mixed with 2.6 mL of cell suspension by vortex for 3 s and its absorbance at 450 nm was immediately collected at 15 s intervals. In the activity assay of adsorbed lysozyme (adsorption at pH 10), 10 mg of MCF–X–Lz (X = OH, C_3H_6H, $C_3H_6NH_2$, $C_3H_6NHCONH_2$, and C_3H_6COOH) was suspended in 100 mL of pH 6.2 buffer by vortex for 5 s. Then 100 μL of MCF–X–Lz solution was immediately taken out and mixed with 2.6 mL of cell suspension. 100 μL of pH 6.2 buffers and 100 μL of MCF–OH solution were used respectively as blank. The lysozyme activity was calculated from the slope of the time course by linear regression of data points. One activity unit (U) is equivalent to an absorbance decrease of 0.001 units/min. The activity of each sample was measured for three times and the results showed good reproducibility.

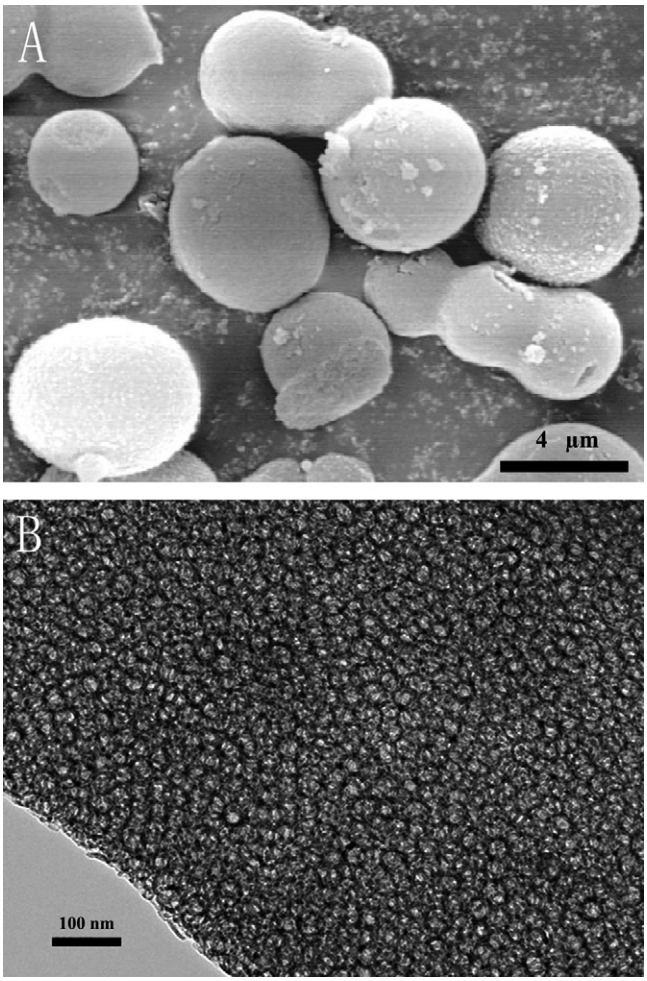

Fig. 1. SEM (A) and TEM (B) images of MCF–OH.

3. Results and discussion

3.1. Adsorbent characterization

MCF was synthesized and then activated using standard activation procedure [36] for silica surface to generate more active silanol groups. Functional group X (X = C_3H_6H, $C_3H_6NH_2$, $C_3H_6NHCONH_2$ and C_3H_6COOH) were selected to modify the silica surface respectively by post-synthesis grafting. The SEM image of MCF–OH (Fig. 1A) displays sphere particles in the majority with 3–5 μm diameters. A minority of ellipsoidal particles with silica bridges could also be observed. The TEM image (Fig. 1B) illustrates ordered cells with uniform diameters of about 20 nm. The MCF materials all show nitrogen sorption isotherms typical of type IV (Fig. 2A). The cell and window size distributions calculated from the adsorption and desorption branch, respectively, are shaped hardly distinctly

Table 1
Textural properties of activated and functionalized MCF materials.

Supports	Specific surface area (m^2/g)	Pore size (nm)		Pore volume (cm^3/g)	The density of functional groups (number/nm^2)
		Cell diameter (nm)	Window diameter (nm)		
MCF–OH	727	17.9	9.7	2.3	4.2
MCF–C_3H_6–H	438	16.7	9.7	1.5	0.8
MCF–C_3H_6–NH_2	423	17.0	9.6	1.5	2.4
MCF–C_3H_6–$NHCONH_2$	285	17.8	7.8	0.8	5.8
MCF–C_3H_6–COOH	521	16.9	9.8	1.8	0.9

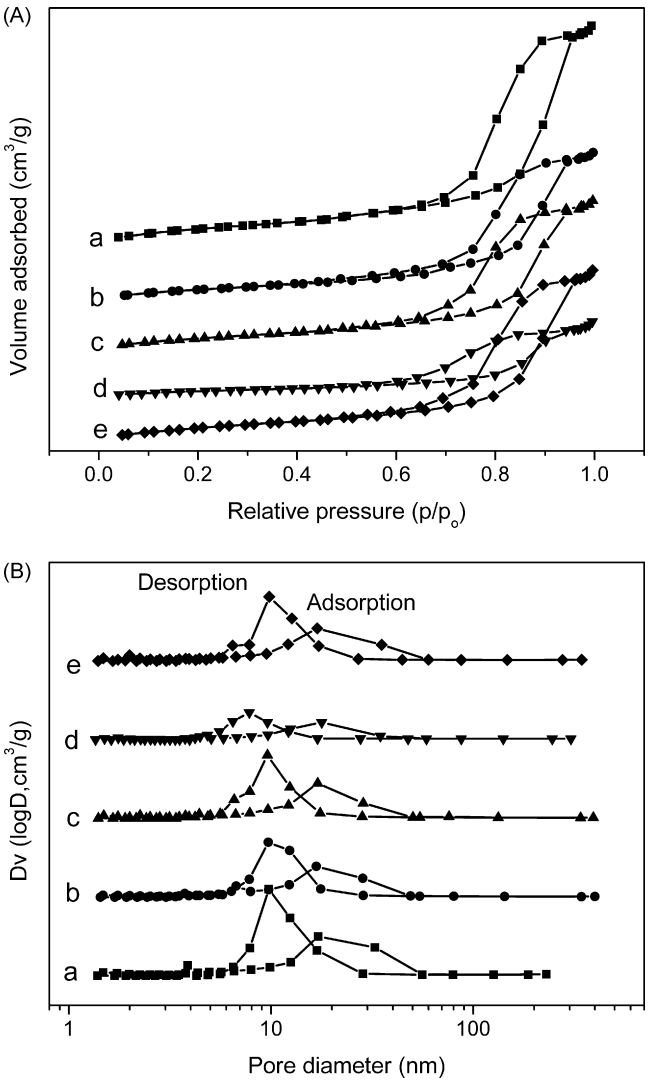

Fig. 2. Nitrogen sorption isotherms (A) and pore size distributions (B) of MCF–OH (a); MCF–C_3H_6H (b); MCF–$C_3H_6NH_2$ (c); MCF–$C_3H_6NHCONH_2$ (d); MCF–C_3H_6COOH (e).

from each other as shown in Fig. 2B. The textural properties of MCF materials are summarized in Table 1. The cell diameter at maximum distribution, calculated as 17.9 nm, is consistent well with observed from TEM image for MCF–OH. The window size of MCF–OH is determined as 9.7 nm. The grafting of functional groups reduces the cell size to around 17.0 nm but makes no obvious effects on the window size of MCF–X except for MCF–$C_3H_6NHCONH_2$. Different from observed for other MCF–X materials, the window diameter of MCF–$C_3H_6NHCONH_2$ decreases by about 2 nm. The observed reductions of surface area, pore volume and pore size of functionalized MCFs are supposed to originate from the attachment of the desired organic groups to the pore surfaces. According to the relative content of Q^2, Q^3, and Q^4 moieties estimated from the integral areas of ^{29}Si MAS NMR signals at −89, −99, and −109 ppm, the molecular formula of MCF–OH is written as $H_{0.3191}O_{2.160}Si$, giving a silanol group density of 4.2 nm^{-2}. Based on the content of nitrogen or carbon (if no nitrogen atom in the grafted functional groups) element, the chain density of surface functional groups was estimated and shown in Table 1. The coverage of –Si–$C_3H_6NHCONH_2$ is estimated to be nearly complete from the chain density, while the coverage of –Si–C_3H_6H and –Si–C_3H_6COOH is lower than 1 taking into consideration that not all silane moieties are grafted to the MCF surface in T^3 linkage. The higher content of functional group in MCF–$C_3H_6NHCONH_2$ accounts for the more loss of surface area and pore volume. The dominating moieties on the surface of functionalized MCF under various pH conditions were analyzed according to p*Ka* of the corresponding functional groups and are shown in Table 2. The surface charge characters of different supports could be further qualitatively determined. The MCF–OH surface is negatively charged and MCF–$C_3H_6NHCONH_2$ surface is positively charged at all pH values investigated. MCF–$C_3H_6NH_2$ surface is positively charged at pH of 4.8 and 6.8 but approaches neutral at pH of 10.0 and 12.0. The MCF–C_3H_6COOH surface is approximately neutral at a pH of 4.8 but negatively charged at higher pH values. The –C_3H_6H group on MCF–C_3H_6H is not charged. But the MCF–C_3H_6H surface might be partially negatively charged because of the residual ungrafted Si–OH.

3.2. Adsorption kinetics of lysozyme on MCF materials

The protein adsorption in nanoporous supports is a complex phenomenon involving multiple steps that occur simultaneously: (1) transport to the surfaces by diffusion, which could be generally enhanced through mixing and shearing action. (2) Pore diffusion, the rate-limiting step when strong interfacial interactions occur (the protein adsorbed to the binding sites remains fixed), and hence mainly depending on the relative size of pores and protein molecules. (3) Adsorption/desorption at the surface, affected by the nature of surface–protein interactions, and described by an interfacial chemical reaction and its related kinetic adsorption and desorption mechanisms. (4) Surface diffusion, influenced mainly by the surface–protein interactions, negligible in the case of strong adsorption (no desorption occurs). (5) Conformational alteration of proteins in contact with the interface, and interactions with other adsorbed protein molecules. As the MCF–X materials involved in this work have similar pore structures, the distinction of adsorption process is supposed to be mainly caused by the occurrence of interfacial interactions. The roles of surface–protein interactions, protein–protein interactions, and conformation alteration of proteins in contact with the interface in the adsorption kinetics are thus to be discussed principally.

Fig. 3 shows the adsorption rate of lysozyme as a function of time on different MCF supports when the silica/lysozyme is 1.5 (w/w) under pH of 4.8, 6.8, 10, and 12, respectively. The kinetic behaviors of lysozyme adsorption are basically similar on different supports under various pH conditions in that they all display distinct stages. In the first stage, the adsorption amount reaches a plateau rapidly

Table 2
Surface moieties of functionalized MCF materials dominant at different pH conditions.

Supports	Functional groups	pH 4.8	pH 6.8	pH 10.0	pH 12.0
MCF–OH	$[-SiO^-]/[-SiOH]$	$10^{1.8}$	$10^{3.8}$	10^{7}	10^{9}
MCF–C_3H_6–NH_2	$[-NH_3^+]/[-NH_2]$	$10^{5.6}$	$10^{3.6}$	$10^{0.37}$	$10^{-1.6}$
MCF–C_3H_6–$NHCONH_2$	$[[-NHCONH_2]H^+]/[-NHCONH_2]$	$10^{9.4}$	$10^{7.4}$	$10^{4.2}$	$10^{2.2}$
MCF–C_3H_6–COOH	$[-COO^-]/[-COOH]$	$10^{0.03}$	10^{2}	$10^{3.2}$	$10^{5.2}$

p*Ka* (Si–OH) = 3.6, p*Ka* (–C_3H_6–COOH) = 4.8, p*Ka* (–C_3H_6–NH_2) = 10.4, p*Ka* (–C_3H_6–$NHCONH_2$) = 14.2.

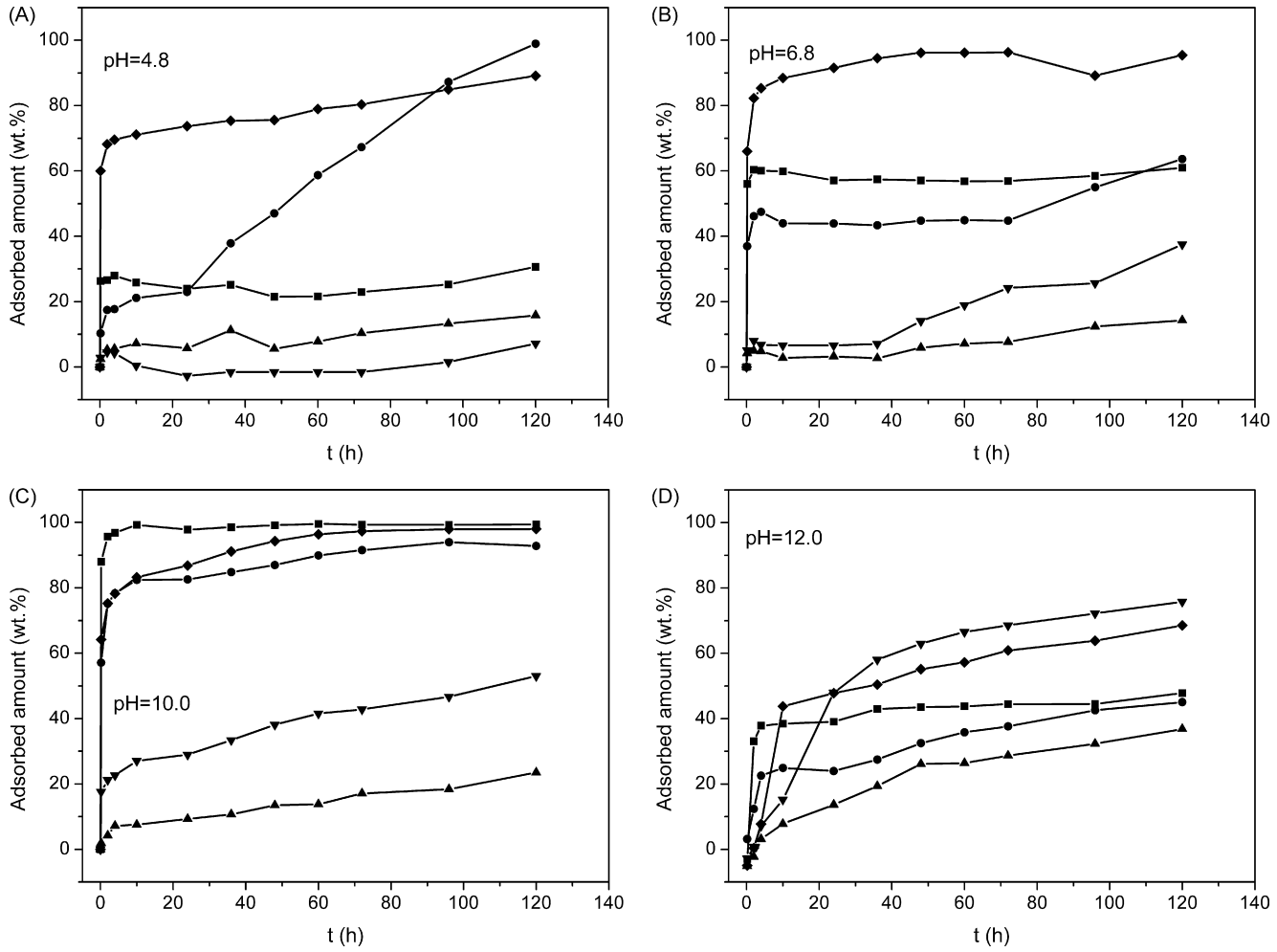

Fig. 3. Adsorption rate of lysozyme at various pH as a function of time on MCF–OH (■); MCF–C_3H_6H (●); MCF–$C_3H_6NH_2$ (▲); MCF–$C_3H_6NHCONH_2$ (▼); MCF–C_3H_6COOH (♦).

generally within 10 h. But the adsorption amount at the plateau (maximal amount achieved in the first stage) exhibits great diversity depending on the surface groups and pH. So does the change trend of adsorption rate in the second stage (after the plateau). At pH 4.8, the lysozyme adsorption on MCF–C_3H_6COOH shows a rapid initial rate indicating high lysozyme-support affinity, and then turns slow. The initial adsorption rate on MCF–C_3H_6H is similar to on MCF–OH. But following the plateau step the adsorption amount on MCF–C_3H_6H exhibits an obvious increase with time. There is almost no impressive adsorption occurring on MCF–$C_3H_6NH_2$ and MCF–$C_3H_6NHCONH_2$. The increase of pH from 4.8 to 6.8 elevates the initial adsorption rates on MCF–OH and MCF–C_3H_6H. A gradual adsorption takes place on MCF–$C_3H_6NHCONH_2$. At pH 10, the lysozyme adsorption on MCF–$C_3H_6NHCONH_2$ exhibits a higher initial rate than observed at lower pH. The adsorption amounts on MCF–$C_3H_6NHCONH_2$ and MCF–$C_3H_6NH_2$ both show gradual increase with time in the second stage. Increasing pH further to 12, the initial adsorption rates on MCF–OH, MCF–C_3H_6H, and MCF–C_3H_6COOH are reduced. But the adsorption on either MCF–$C_3H_6NH_2$ or MCF–$C_3H_6NHCONH_2$ is improved. The initial adsorption amount on MCF–$C_3H_6NHCONH_2$ even becomes the highest one, different from observed under other pH. Except for on MCF–OH, the adsorption on each support occurs continuously following the initial stage. The observed difference in the initial adsorption rate should be well explained by the nature of the interfacial surface–protein interactions predicted in Table 3. The charge repulsion results in slower adsorption rate, while either charge attraction, hydrophobic interaction, or certain hydrogen bonding serve as driving forces for lysozyme adsorption, as can be clearly observed in Fig. 3. It is surprising that the hydrogen bonding between surface –$C_3H_6NH_2$ and lysozyme seems not strong enough to efficiently drive lysozyme adsorption. At pH 12, the

Table 3
Theoretical analysis of possible surface–protein interactions dominant at various pH conditions on different supports[a].

pH	MCF–OH	MCF–C_3H_6–H	MCF–C_3H_6–NH_2	MCF–C_3H_6–$NHCONH_2$	MCF–C_3H_6–COOH
4.8	Charge attraction	Hydrophobic affinity	Charge repulsion	Charge repulsion + π–π overlap	Hydrogen bonding + charge attraction
6.8	Charge attraction	Hydrophobic affinity	Charge repulsion	Charge repulsion + π–π overlap	Charge attraction
10.0	Charge attraction	Hydrophobic affinity	Hydrogen bonding + charge repulsion	Charge repulsion + π–π overlap	Charge attraction
12.0	Charge repulsion	Hydrophobic affinity	Hydrogen bonding	Charge attraction + π–π overlap	Charge repulsion

[a] Based on the charge characters of support surfaces shown in Table 2 and lysozyme. The net charges of lysozyme molecules at pH 4.8, 6.8, 10, and 12 is +10, +8, +6, and −4, respectively, according to Ref. [50].

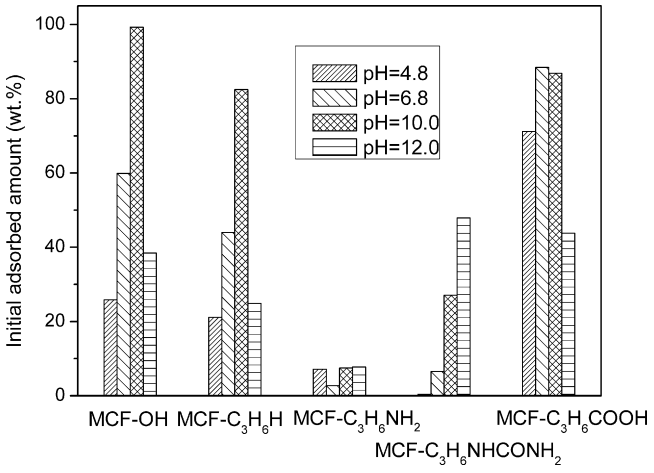

Fig. 4. Dependence of initial adsorption amount on pH.

adsorption rate on MCF–$C_3H_6NH_2$ is even slower than on MCF–OH and MCF–C_3H_6COOH where charge repulsion exists.

The dependence of initial adsorption rate on the nature of surface–protein interfacial interaction is observed more clearly in Fig. 4. It can be seen from Fig. 4 that the initial adsorption rate increases along with pH for MCF–C_3H_6NHCONH$_2$ and changes hardly for MCF–$C_3H_6NH_2$, while shows maximums for other supports. As shown in Table 3, the dominant interfacial interaction for MCF–OH and lysozyme is the electrostatic attraction between negatively charged surface and positively charged protein at a pH lower than 11 (pI of Lz), and then turns to electrostatic repulsion at pH 12. As a result, the initial adsorption rate on MCF–OH displays a decrease when the adsorption pH increases from 10 to 12. Similar is the initial adsorption rate on MCF–C_3H_6COOH. In the MCF–C_3H_6COOH and lysozyme system, the dominant surface–protein interaction transforms from hydrogen bonding at pH 4.8 to charge attraction at pH 6.8 and 10, and finally to charge repulsion at pH 12. The change of initial adsorption rate with pH on MCF–C_3H_6H is similar to MCF–OH. The observed similarity originates from the interference of electrostatic forces because the coverage of –C_3H_6H is much less than 1. For MCF–C_3H_6NHCONH$_2$, the surface–protein electrostatic repulsion dominates at pH 4.8 and 6.8, resulting in similar slow adsorption rates. Although the surface-protein charge repulsion is still present at pH 10, the π–π overlapping between the –NHCO– moiety in –C_3H_6NHCONH$_2$ group and the peptide bonds in proteins becomes dominant, resulting in a distinct increase in the initial adsorption rate. The surface charge of lysozyme decreases at a pH close to pI, which causes the weakening of the surface–protein charge repulsion. The affinity between the MCF–C_3H_6NHCONH$_2$ surface and lysozyme is, therefore, strong enough to counteract the charge repulsion at pH 10. The charge attraction of surface–protein contributes to the further increase in adsorption rate at pH 12. For MCF–$C_3H_6NH_2$, although the surface–protein interaction transforms from charge repulsion to hydrogen bonding at pH ≥ 10, no obvious increase in initial adsorption rate is observed, which implies that the hydrogen bonding between lysozyme and MCF–$C_3H_6NH_2$ is not sufficient or strong enough to drive lysozyme adsorption.

The support–protein interactions predicted according to the charge characters of support and lysozyme surfaces (Table 3) well account for the dependence of adsorption kinetics on pH. But it has to be noted that the initial adsorption rates on MCF–OH at pH 4.8 is an exception. As can be observed from Fig. 4, the adsorption rate on MCF–OH (MCF–C_3H_6H alike) is severely influenced by the adsorption pH even when the nature of surface–protein interaction is the same electrostatic attraction. The adsorption rate at pH 4.8 is much slower than pH 10. This kind of pH effects is consistent with reported previously by Vinu et al. [15,24]. They proposed that the lateral repulsion between lysozyme molecules greatly reduce the adsorption amount. It has been reported that the area per molecule of lysozyme in solution having a pH near the isoelectric point is similar to that in its crystallized state (13.5 nm^2), whereas it doubles to 26.6 nm^2 in a solution pH of 4 [40]. The adsorption rate on MCF–OH decreases by more than one half when pH changes from 10 to 4.8 as shown in Fig. 4. However, this pH effect appears more evident when the surface–protein charge attraction predominates. On MCF–C_3H_6COOH where hydrogen bonding additionally contributes to the lysozyme adsorption, the dependence of adsorption rate on pH gets lessened. The initial adsorption rate changes hardly with pH on MCF–$C_3H_6NH_2$ where Van der Waals (hydrogen bonding) is dominant for driving force. This dependent role of protein–protein lateral repulsion in the adsorption could rationally be explained by the surface diffusion of lysozyme. Moreover, the surface diffusion and protein–protein repulsion could also account for the adsorption amount change following the initial adsorption in Fig. 3. When the surface–protein interaction is stronger, electrostatic force for example, the surface diffusion of the protein already adsorbed is slowed down, or even no surface diffusion occurs. So no slow adsorption is clearly observed. But when the Van der Waals force is involved in the adsorption, the surface diffusion of protein gets easier. The slow adsorption proceeding from the surface diffusion of protein explains the observed gradual increase in the adsorption amount following the initial rapid adsorption.

3.3. Adsorption equilibrium of lysozyme on MCF materials

The adsorption isotherms determined at pH 6.8 and 10 are illustrated in Figs. 5 and 6, respectively. As shown in Fig. 5, the adsorption isotherms of lysozyme at pH 6.8 on MCF–OH, MCF–C_3H_6H, and MCF–C_3H_6COOH display L-type characteristic of a high affinity between lysozyme and the adsorbent surface. The high surface–protein affinity results in a sharp initial rise of adsorption amount. The adsorption on MCF–$C_3H_6NH_2$ or MCF–C_3H_6NHCONH$_2$ shows an S-type isotherm typical of weak surface–protein affinity, consistent with the fact that the charge repulsion predominates over the surface–protein interactions. When increasing the adsorption pH from 6.8 to 10, the adsorption

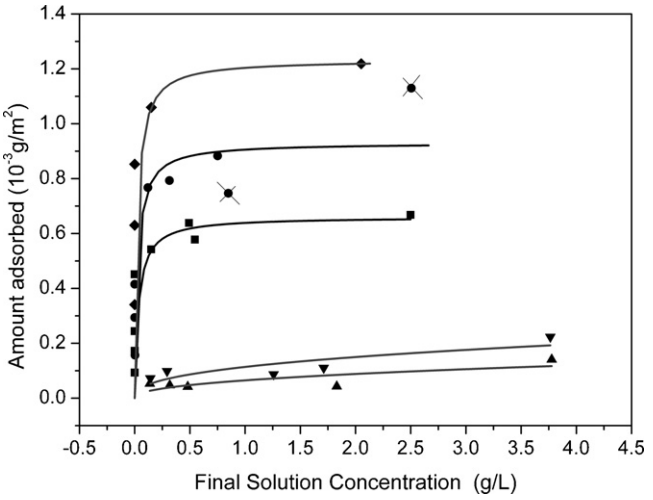

Fig. 5. Adsorption isotherms of lysozyme at pH 6.8 and T = 298 K on MCF–OH (■); MCF–C_3H_6H (●); MCF–$C_3H_6NH_2$ (▲); MCF–C_3H_6NHCONH$_2$ (▼); MCF–C_3H_6COOH (♦).

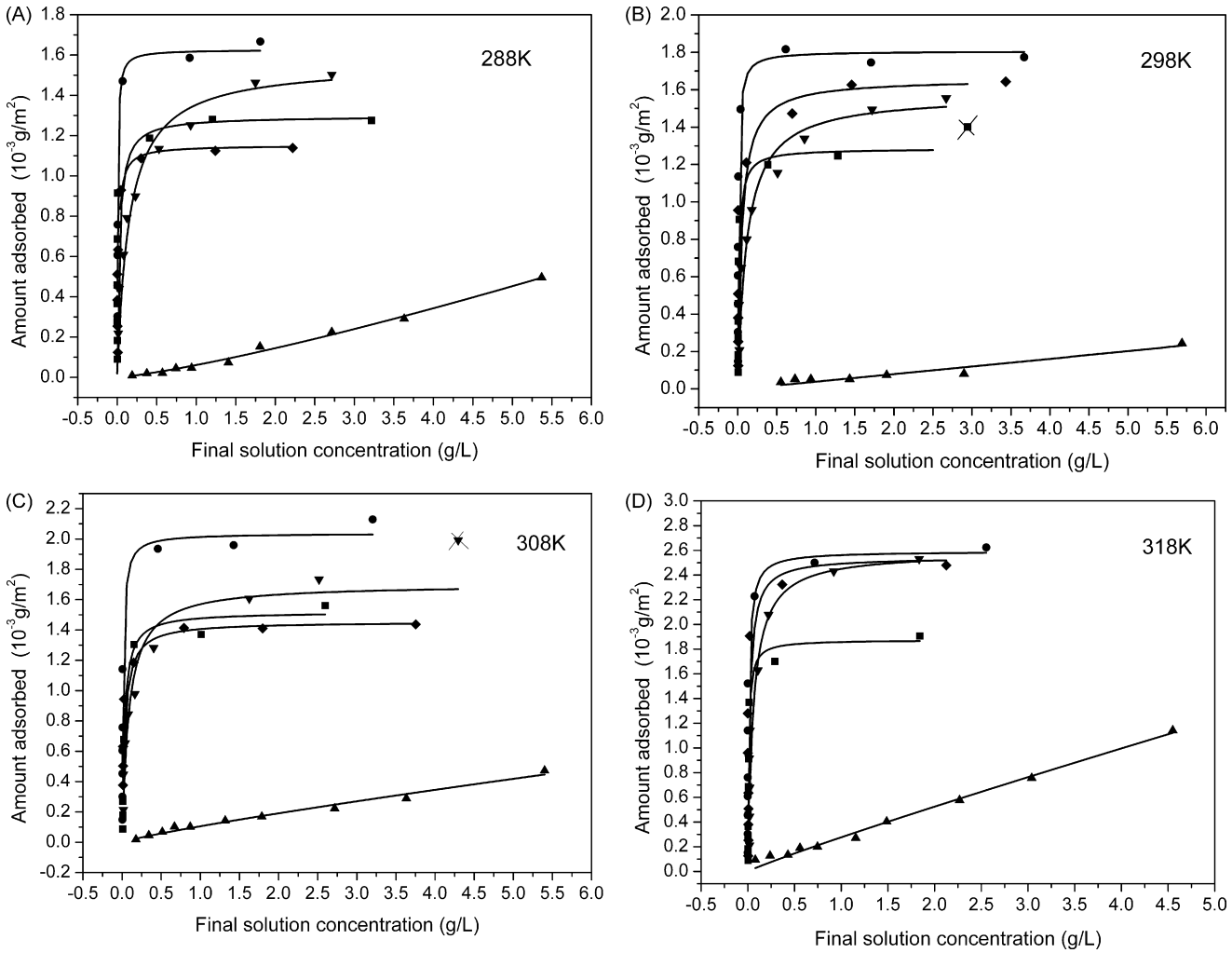

Fig. 6. Adsorption isotherms of lysozyme at pH 10 on MCF–OH (■); MCF–C_3H_6H (●); MCF–$C_3H_6NH_2$ (▲); MCF–$C_3H_6NHCONH_2$ (▼); MCF–C_3H_6COOH (♦) at T = 288, 298, 308 and 318 K, respectively.

isotherm on MCF–$C_3H_6NHCONH_2$ changes to an L-type displaying a sharp initial rise (Fig. 6), in accordance with the transformation of surface–protein repulsion to high affinity by π–π overlapping. Although the surface–protein interaction turns to hydrogen bonding from charge repulsion for MCF–$C_3H_6NH_2$, the adsorption isotherm still shows an S-type representing a weak surface–protein affinity. For MCF–OH, MCF–C_3H_6H and MCF–C_3H_6COOH, the quasi-steady adsorption amounts increase with pH changed from 6.8 to 10 due to the reduction of protein–protein repulsions.

As can be distinguished from Fig. 6, the lysozyme adsorption on MCF–$C_3H_6NHCONH_2$ is difficult to achieve a steady state in comparison with the adsorption on other supports. This is probably due to the roles of dependent conformational alteration of proteins. It is well known that the π–π overlapping is more orientational and direction-selective than electrostatic force, hydrophobic interaction and hydrogen bonding. The occurrence of π–π overlapping requires oriented close-up or contact of proteins to support surfaces. To be adsorbed by π–π overlapping, the proteins have to experience conformational change on the surface, accounting for the prolongation of adsorption equilibrium on MCF–$C_3H_6NHCONH_2$.

Describing the L-type isotherms by pseudo-Langmuir sorption model (1) [24] and S-type isotherm by Freundlich model (2), the fitting plots are shown in Fig. 5 and Fig. 6 together with experimental data points:

$$\frac{\Gamma}{\Gamma \mathrm{m}} = \frac{K_L C}{1 + K_L C} \tag{1}$$

$$\Gamma = K_F C^{1/n} \tag{2}$$

wherein K_L and K_F are Langmuir and Freundlich parameters, respectively, C is the lysozyme concentration in solution, Γ_m is the monolayer adsorption capacity, Γ is the adsorbed amount determined experimentally, and n is non-linear coefficient. From the simulated plots, the corresponding parameters are estimated and given in Tables 4 and 5. Generally, the experimental points at pH 10 are fitted better than at pH 6.8. The experimental points for MCF–OH, MCF–C_3H_6H, and MCF–C_3H_6COOH at pH 10 are described by Langmuir equation better than for MCF–$C_3H_6NHCONH_2$. The deviation of simulated Langmuir plots from experimental data at high coverage for MCF–$C_3H_6NHCONH_2$ is attributed to the adsorption retardation by lysozyme conformational alterations. Because the adsorbed amount continuously changes with time without exhibiting a clear plateau in some cases (as can be seen in Fig. 3), a genuine steady state is hard to reach. So the Γ_m is actually an adsorbed amount in quasi-steady state where the change of adsorbed amount with time or lysozyme concentration turns into gentle. As shown in Tables 4 and 5, elevating the adsorption pH from

Table 4
Langmuir and Freundlich constants for adsorption isotherms at 298 K at pH 6.8.

Supports	Langmuir model		
	Γ_m ($\times10^{-3}$ g m^{-2})	K_L (L g^{-1})	R^2
MCF–OH	0.66	29.00	0.7306
MCF–C_3H_6–H	0.85	83.08	0.9914
MCF–C_3H_6–COOH	1.23	40.66	0.8349

Supports	Freundlich model		
	K_F	n	R^2
MCF–C_3H_6–NHCONH$_2$	0.114	2.529	0.6888
MCF–C_3H_6–NH$_2$	0.052	1.519	0.7113

6.8 to 10, the quasi-steady adsorption amounts increase obviously. But the increments for MCF–OH and MCF–C_3H_6H are higher than for MCF–C_3H_6COOH. The observations, quite similar to the change of initial adsorption rate with pH on the corresponding support, illuminates that the biomimetic modification of inorganic surface counteracts partly the inhibition effect of protein–protein lateral repulsion on the adsorption. The parameters K_L or K_F at 288, 298, 308, and 318 K are also estimated from the sorption isotherms at pH 10 (Fig. 6) and given in Table 5.

Besides advanced techniques like calorimetry, microcalorimetry, mass spectrophotometry and photon correlation spectroscopy for thermodynamic studies [32], the classical van't Hoff equation (3) could also be used in a certain temperature range to calculate the thermodynamic parameters. The enthalpy and entropy alterations for interfacial interaction could be obtained by linearly plotting the logarithm of the equilibrium constant with inversed temperature. Non-linear van't Hoff behavior often occurs in the protein adsorption. The non-linearity is in part due to the protein structure change, which results in an increase in the conformational entropy at higher temperatures [41]. In this work, the resulting $\ln K_L$ (or $\ln K_F$) shows a good linear relationship with $1/T$ maybe due to the good thermostability of lysozyme. The denaturation temperature of lysozyme is 72 °C and the lysozyme secondary structure is kept unchanged till about 60 °C according to the investigation by circular dichroism spectra [42]:

$$\ln K = \frac{\Delta S}{R} - \frac{\Delta H}{RT} \quad (3)$$

The ΔH_{ads} in the lysozyme sorption on various supports accords well with the nature of surface-protein interaction. The high affinity of MCF–OH, MCF–C_3H_6H or MCF–C_3H_6COOH to lysozyme results in an exothermic sorption, while the adsorption of lysozyme on MCF–C_3H_6NHCONH$_2$ and MCF–C_3H_6NH$_2$ appears endothermic. But all the thermal effects are feeble as a result of non-covalent surface–protein interactions. The negative ΔS indicates a slight increase in the system order after surface–protein binding. For MCF–C_3H_6NHCONH$_2$ and MCF–C_3H_6NH$_2$, the entropy increase may result from the gain in configurational entropy for the formation of orientational π–π overlapping and dehydrating apolar patches on the lysozyme surface due to protein aggregates [39].

It is interesting to note that the hydrophobic affinity, π–π overlapping, and hydrogen bonds exhibit great difference in driving lysozyme adsorption, although they are all Van der Waals. The hydrophobic affinity, π–π overlapping, and the hydrogen bonding between –C_3H_6COOH and lysozyme favor the lysozyme adsorption concerning both of the adsorption kinetics and sorption isotherms. But the hydrogen bonding between MCF–C_3H_6NH$_2$ surface and lysozyme work less on the lysozyme adsorption. The significant role of π–π overlapping could rationally be associated with the extensive presence of peptide linkages on lysozyme surface. The hydrophobic affinity enough to drive the adsorption of lysozyme on MCF–C_3H_6H could be related to the appropriately hydrophobic lysozyme surface. The general distribution of side chains in protein usually conforms closely to the pattern observed in myoglobin in that all of the ionizable groups and most of the polar side chains are distributed over the molecule surface, while the majority of the apolar side chains lie within its interior [43]. But for most small globular proteins, the apolar atoms occupy between 40 and 60% of the water-accessible surface area, which gives the proteins relatively high surface hydrophobicity [43]. For lysozyme, the

Table 5
Langmuir and Freundlich constants for adsorption isotherms at different temperatures at pH 10 and the thermodynamic parameters for protein adsorption.

Supports	T (K)	Langmuir model			ΔH_{ads} (kJ mol^{-1})	ΔS_{ads} (J mol^{-1} K^{-1})	R
		Γ_m ($\times10^{-3}$ g m^{-2})	K_L (L g^{-1})	R^2			
MCF–OH	288	1.29	65.00	0.8535	−18	−29	0.9146
	298	1.29	61.30	0.9117			
	308	1.52	34.95	0.9040			
	318	1.92	35.59	0.9649			
MCF–C_3H_6–H	288	1.63	173.73	0.9844	−19	−24	0.9456
	298	1.81	112.83	0.8894			
	308	2.04	85.39	0.8834			
	318	2.59	83.82	0.9472			
MCF–C_3H_6–NHCONH$_2$	288	1.56	6.59	0.9442	+25	+102	−0.9798
	298	1.57	8.65	0.9244			
	308	1.70	11.86	0.9365			
	318	2.59	17.68	0.9072			
MCF–C_3H_6–COOH	288	1.15	70.22	0.9208	−11	−3	0.9587
	298	1.56	67.04	0.8518			
	308	1.42	51.25	0.9467			
	318	2.55	47.39	0.8962			

Supports	T (K)	Freundlich model			ΔH_{ads} (kJ mol^{-1})	ΔS_{ads} (J mol^{-1} K^{-1})	R
		K_F	n	R^2			
MCF–C_3H_6–NH$_2$	288	0.051	0.739	0.9930	+43	+123	−0.9307
	298	0.054	0.858	0.9227			
	308	0.105	1.168	0.9809			
	318	0.276	1.081	0.9892			

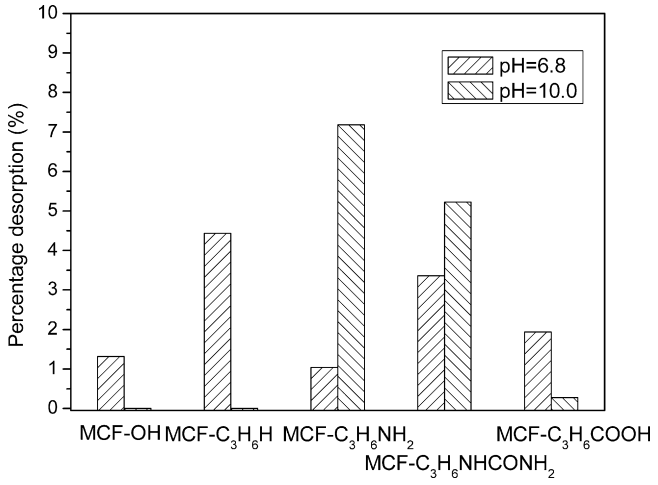

Fig. 7. Partial reversibility of lysozyme adsorption on different supports.

apolar residues cover 59% [44] of the protein surface, which consists of hydrophobic tryptophan, isolcuci, and valine residues [45]. The hydrogen bonding interaction between the terminal $-NH_2$ on support surface and polar arginine and lysine residues [45] on the exterior surface of lysozyme seems relatively difficult, resulting in a less affinity and a slower initial adsorption rate.

3.4. Distribution and adsorption reversibility of lysozyme on MCF materials

According to the sorption isotherms discussed above, the distribution states of lysozyme on the supports with different surface modifications are depicted as follows. Lysozyme is distributed on MCF–$C_3H_6NH_2$ in protein aggregates at either pH 6.8 or 10, while in monolayer on MCF–OH, MCF–C_3H_6H, and MCF–C_3H_6COOH. The density of lysozyme in monolayer increases with pH on MCF–OH, MCF–C_3H_6H, and MCF–C_3H_6COOH. The lysozyme on MCF–$C_3H_6NHCONH_2$ transforms from multilayer aggregate to monolayer distribution as pH increases.

The lysozyme molecules adsorbed at pH 6.8 and 10 on the MCF supports with different surface modifications were leached in buffer to investigate the adsorption reversibility. The observed percentage desorption in each case indicates the adsorption of lysozyme is only partially reversible. The lysozyme is leached in a ratio of less than 8%, as shown in Fig. 7. Under the same adsorption and desorption condition, the percentage desorption ratio of lysozyme in the tested candidates shows a little diversity depending on the distribution states, surface–protein interactions, as well as protein–protein interactions. Generally, the lysozyme adsorbed in multilayer aggregate is more readily to be leached. For example, the lysozyme adsorbed on MCF–$C_3H_6NH_2$ at pH 10 shows the highest percentage desorption. The existence of charge repulsion between MCF–$C_3H_6NHCONH_2$ and lysozyme results in higher desorption. Although lysozyme is all distributed in monolayer on MCF–OH, MCF–C_3H_6H, and MCF–C_3H_6COOH at pH 6.8 and 10, the adsorption at pH 6.8 is more reversible because of the larger contribution of protein–protein repulsion. Relatively high is the percentage desorption on MCF–C_3H_6H at pH 6.8, where the protein–protein repulsion rivals the surface–protein hydrophobic affinity.

3.5. FT-IR investigation of lysozyme secondary structure

Infrared spectroscopy is a useful technique to monitor the structural changes when the proteins were immobilized on the supports [46]. The amide I band (1600–1700 cm^{-1}) arises from the α-helix, β-sheet, β-turn, and random coil in protein conformation. The amide II band (1500–1600 cm^{-1}) is related to a combination of C–N stretching and N–H bending vibrations of the protein backbone. Both of amide I and II image the secondary structure of proteins [24,47]. Fig. 8 shows the FT-IR spectra of lysozyme adsorbed on the functionalized MCF supports. For comparison, the spectra for pristine support and lysozyme are also illustrated. The IR bands characteristic of amide I and II are clearly observed at 1652 and 1536 cm^{-1}, respectively. The shift of 1536–1558 cm^{-1} observed on either MCF–$C_3H_6NHCONH_2$ or MCF–C_3H_6COOH is supposed to originate from the interference of $-NHCONH_2$ and $-COO^-$ groups on MCF surfaces. The $-NHCONH_2$ has IR absorptions at 1650 and 1558 cm^{-1}. The envelope of surface $-NHCONH_2$ absorption causes the observed shift. The deprotonization of –COOH in the adsorption (pH 10) shifts its absorption from 1718 to 1610–1560 cm^{-1}. The resulting strong absorption covers the information of amide II of protein. To discuss the structural changes quantitatively, curve-fitting was performed on the FT-IR bands in amide I regions. The curve-fitting results are shown in Fig. 8 (right). Because of the interference of $-COO^-$ and $-NHCONH_2$ groups, the curve-fitting was only performed on the lysozyme native and adsorbed on MCF–OH, MCF–C_3H_6H and MCF–$C_3H_6NH_2$. In comparison to native lysozyme, the adsorption causes a negligible change in the contents of α-helix and β-sheet (within 2%), indicating that the secondary structure of lysozyme is well retained. This is consistent with previous results by hydrogen–deuterium exchange combined with mass spectrometry (HDX–MS) and differential scanning calorimetry (DSC) experiments [48]. It has been suggested [39,49] that soft proteins such as bovine serum albumin (BSA) and immunoglobulin G (lgG) unfold partially upon adsorption, while lysozyme, which has a much stronger inter coherence (hard protein), shows less structural alteration.

3.6. Activity investigation of lysozyme

The enzymatic activity of lysozyme was investigated using the standard kinetic lysis of *M. lysodeikticus* cells by measuring the turbidity decrease [35]. Measurement of the absorbance at 450 nm (A450) was taken for 20 min at 15 s intervals and the collected values were plotted as a function of time (Fig. 9). The activity of lysozyme was calculated from the slope of the linear regression. As shown in Fig. 9, the cell suspension without lysozyme introduced (curve f for buffer and curve g for MCF–OH) shows no change during the 20-min measurement course. The decrease in A450 for native lysozyme (Lz) is linear in the initial 180 s. For the immobilized lysozyme, all the curves (curve a, b, d and e) except that for MCF–$C_3H_6NH_2$–Lz (curve c) show reverse S-shape. The slow decrease in A450 in the first 3–4 min is related to the diffusion process of lysozyme from the MCF surface to cell solution. The activity should be calculated from linear regression in the following 180 s. From the A450 versus time curves, the expressed activities (U/mg MCF-X-Lz) were estimated (shown in Fig. 9) well consistent with the adsorption amount of lysozyme on the corresponding supports at pH 10. The relative activity, defined the ratio of the specific activity (U/mg Lz) of adsorbed lysozyme to the specific activity of native lysozyme, are 100%, 96%, 95% and 96%, respectively, for MCF–OH–Lz, MCF–C_3H_6H–Lz, MCF–$C_3H_6NHCONH_2$–Lz, and MCF–C_3H_6COOH–Lz, meaning that lysozyme keeps full activity in the adsorption–desorption–catalytic process. For MCF–$C_3H_6NH_2$–Lz, the absorbance shows almost no change (curve c), which is supposed to result from the low lysozyme adsorption amount and low percentage desorption (<1% at pH 6.2).

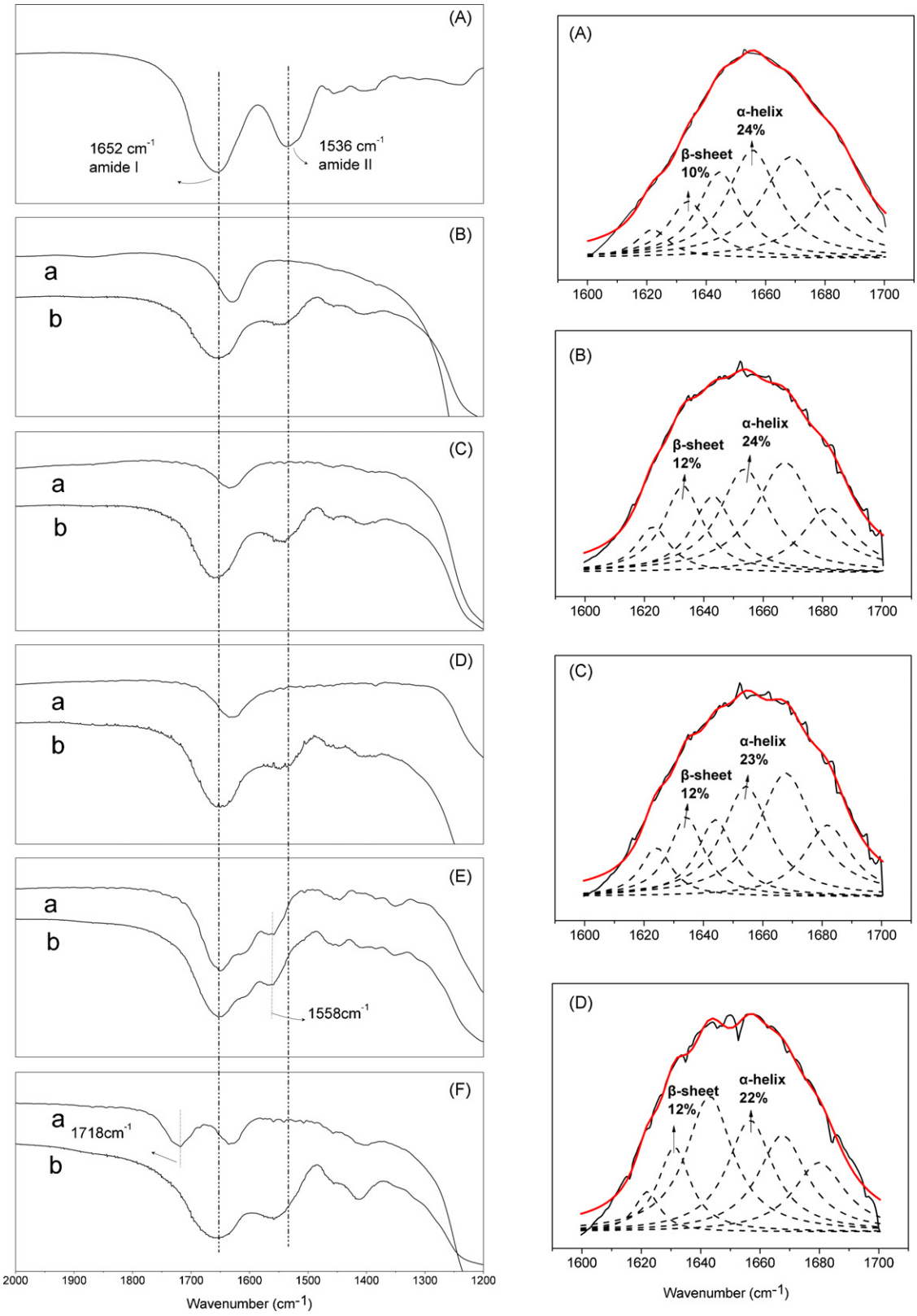

Fig. 8. FT-IR spectra of lysozyme powder (A) and MCF–OH (B); MCF–C_3H_6H (C); MCF–$C_3H_6NH_2$ (D); MCF–$C_3H_6NHCONH_2$ (E); MCF–C_3H_6COOH (F), without (a) and with (b) lysozyme adsorbed. The corresponding Lorentz curve-fitting of the spectra in the amide I region are given on the right. The dashed peaks represent the individual Lorents bands.

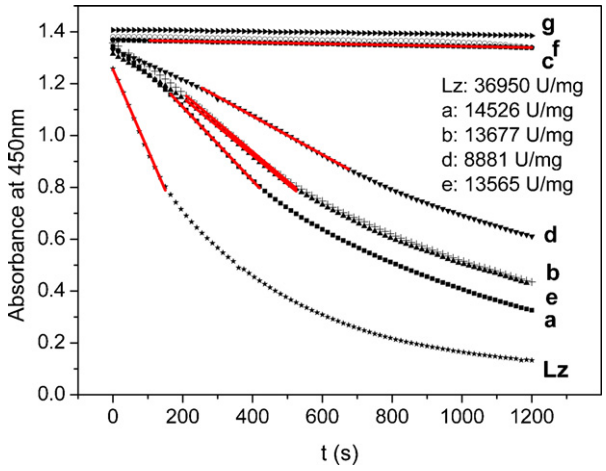

Fig. 9. The absorbance changes at 450 nm with the time of cell solution in the presence of native lysozyme (Lz); MCF–OH–Lz (a); MCF–C_3H_7–Lz (b); MCF–$C_3H_6NH_2$–Lz (c); MCF–$C_3H_6NHCONH_2$–Lz (d); MCF–C_3H_6COOH–Lz (e); buffer only (f) and MCF–OH (g).

4. Conclusion

In summary, the adsorption characteristics of lysozyme on MCF materials have been investigated by tuning the non-covalent interfacial interactions through biomimetic modification of inorganic surfaces. The adsorption rate and adsorption capacity depend mainly on the nature of protein–support interfacial interactions. The protein–protein repulsions make impact on the lysozyme adsorption not independently of surface–protein interactions. It is worthy to note that the biomimetic modification of inorganic support surface counteracts in part the inhibition effects of protein–protein repulsion on protein adsorption, thus favoring the adsorption capacity. The non-orientational interfacial forces make for easier achievement of quasi-steady state or quasi equilibrium in adsorption isotherms. The lysozyme adsorption on modified MCFs is partially reversible, making no damage on the protein secondary structure and enzymatic activity, which is preferred by the applications in bio-catalysis, protein separation, and bio-sensing. Our findings in this work are believed to provide great insights for tuning protein adsorption heterogeneities, which is significantly crucial to generate the desired adsorption for protein immobilization, bioreactors, bio-sensors, or bio-separation.

Acknowledgments

The authors are grateful to the financial support from NSFC, 973 project (2009CB939802), Program for New Century Excellent Talents in University (NCET), and “111” Project.

References

[1] C.T. Kresge, M.E. Leonowicz, W.J. Roth, J.C. Vartuli, J.S. Beck, Ordered mesoporous molecular sieves synthesized by a liquidcrystal template mechanism, Nature 359 (1992) 710–712.
[2] J.S. Beck, J.C. Vartuli, W.J. Roth, M.E. Leonowicz, C.T. Kresge, K.D. Schmitt, C.T.W. Chu, D.H. Olson, E.W. Sheppard, S.B. McCullen, J.B. Higgins, J.L. Schlenker, A new family of mesoporous molecular sieves prepared with liquid crystal templates, J. Am. Chem. Soc. 114 (1992) 10834–10843.
[3] S.A. Bagshaw, E. Prouzet, T.J. Pinnavaia, Templating of mesoporous molecular sieves by nonionic polyethylene oxide surfactants, Science 269 (1995) 1242–1244.
[4] Q. Huo, R. Leon, P.M. Petroff, G.D. Stucky, Mesostructure design with gemini surfactants: supercage formation in a three-dimensional hexagonal array, Science 268 (1995) 1324–1327.
[5] P.T. Tanev, T.J. Pinnavaia, A neutral templating route to mesoporous molecular sieves, Science 267 (1995) 865–867.
[6] D. Zhao, J. Feng, Q. Huo, N. Melosh, G.H. Fredrickson, B.F. Chmelka, G.D. Stucky, Triblock copolymer syntheses of mesoporous silica with periodic 50 to 300 angstrom pores, Science 279 (1998) 548–552.
[7] P. Schmidt-Winkel, W.W. Lukens, D. Zhao, P. Yang, B.F. Chmelka, G.D. Stucky, Mesocellular siliceous foams with uniformly sized cells and windows, J. Am. Chem. Soc. 121 (1999) 254–255.
[8] J.F. Diáz, K.J. Balkus Jr., Enzyme immobilization in MCM-41 molecular sieve, J. Mol. Catal. B: Enzyme 2 (1996) 115–126.
[9] H.H.P. Yiu, P.A. Wright, N.P. Botting, Enzyme immobilisation using siliceous mesoporous molecular sieves, Micropor. Mesopor. Mater. 44–45 (2001) 763–768.
[10] M. Hartmann, Ordered mesoporous materials for bioadsorption and biocatalysis, Chem. Mater. 17 (2005) 4577–4593.
[11] Y. Han, G.D. Stucky, A. Butler, Mesoporous silicate sequestration and release of proteins, J. Am. Chem. Soc. 121 (1999) 9897–9898.
[12] H.H.P. Yiu, C.H. Botting, N.P. Botting, P.A. Wright, Size selective protein adsorption on thiol-functionalised SBA-15 mesoporous molecular sieve, Phys. Chem. Chem. Phys. 3 (2001) 2983–2985.
[13] J. Deere, E. Magner, J.G. Wall, B.K. Hodnett, Mechanistic and structural features of protein adsorption onto mesoporous silicates, J. Phys. Chem. B 106 (2002) 7340–7347.
[14] J. Fan, J. Lei, L. Wang, C. Yu, B. Tu, D. Zhao, Rapid and high-capacity immobilization of enzymes based on mesoporous silicas with controlled morphologies, Chem. Commun. 3 (2003) 2140–2141.
[15] A. Vinu, V. Murugesan, O. Tangermann, M. Hartmann, Adsorption of cytochrome c on mesoporous molecular sieves: influence of pH, pore diameter, and aluminum incorporation, Chem. Mater. 16 (2004) 3056–3065.
[16] A. Katiyar, N.G. Pinto, Visualization of size-selective protein separations on spherical mesoporous silicates, Small 2 (2006) 644–648.
[17] J. Liu, C. Li, Q. Yang, J. Yang, C. Li, Morphological and structural evolution of mesoporous silicas in a mild buffer solution and lysozyme adsorption, Langmuir 23 (2007) 7255–7262.
[18] J.M. Kisler, A. Dahler, G.W. Stevens, A.J. O'Connor, Separation of biological molecules using mesoporous molecular sieves, Micropor. Mesopor. Mater. 44–45 (2001) 769–774.
[19] Y. Kang, J. He, X. Guo, X. Guo, Z. Song, Influence of pore diameters on the immobilization of lipase in SBA-15, Ind. Eng. Chem. Res. 46 (2007) 4474–4479.
[20] A. Salis, D. Meloni, S. Ligas, M.F. Casula, M. Monduzzi, V. Solinas, E. Dumitriu, Physical and chemical adsorption of Mucor javanicus lipase on SBA-15 mesoporous silica. Synthesis, structural characterization, and activity performance, Langmuir 21 (2005) 5511–5516.
[21] K. Muller-Dethlefs, P. Hobza, Noncovalent interactions: a challenge for experiment and theory, Chem. Rev. 100 (2000) 143–168.
[22] A. Sadana, Protein adsorption and inactivation on surfaces. Influence of heterogeneities, Chem. Rev. 92 (1992) 1799–1818.
[23] S. Hudson, E. Magner, J. Cooney, B.K. Hodnett, Methodology for the immobilization of enzymes onto mesoporous materials, J. Phys. Chem. B 109 (2005) 19496–19506.
[24] A. Vinu, V. Murugesan, M. Hartmann, Adsorption of lysozyme over mesoporous molecular sieves MCM-41 and SBA-15: influence of pH and aluminum incorporation, J. Phys. Chem. B 108 (2004) 7323–7330.
[25] Y. Wang, F. Caruso, Mesoporous silica spheres as supports for enzyme immobilization and encapsulation, Chem. Mater. 17 (2005) 953–961.
[26] A. Katiyar, L. Ji, P. Smirniotis, N.G. Pinto, Protein adsorption on the mesoporous molecular sieve silicate SBA-15: effects of pH and pore size, J. Chromatogr. A 1069 (2005) 119–126.
[27] G. Yin, Z. Liu, J. Zhan, F. Ding, N. Yuan, Impacts of the surface charge property on protein adsorption on hydroxyapatite, Chem. Eng. J. 87 (2002) 181–186.
[28] C. Lei, Y. Shin, J. Liu, E.J. Ackerman, Entrapping enzyme in a functionalized nanoporous support, J. Am. Chem. Soc. 124 (2002) 11242–11243.
[29] A.S.M. Chong, X.S. Zhao, Functionalized nanoporous silicas for the immobilization of penicillin acylase, Appl. Surf. Sci. 237 (2004) 398–404.
[30] S. Duinhoven, R. Poort, G.V. Voet, W.G.M. Agterof, W. Norde, J. Lyklema, Driving forces for enzyme adsorption at solid–liquid interfaces, J. Colloid Interface Sci. 170 (1995) 340–350.
[31] M. Rabe, D. Verdes, M. Rankl, G.R.J. Artus, S. Seeger, A comprehensive study of concepts and phenomena of the nonspecific adsorption of β-lactoglobulin, ChemPhysChem 8 (2007) 862–872.
[32] S.K. Parida, S. Dash, S. Patel, B.K. Mishra, Adsorption of organic molecules on silica surface, Adv. Colloid Interface Sci. 121 (2006) 77–110.
[33] Y. Han, J.T. Watson, G.D. Stucky, A. Butler, Catalytic activity of mesoporous silicate-immobilized chloroperoxidase, J. Mol. Catal. B: Enzyme 17 (2002) 1–8.
[34] Y. Han, S.S. Lee, J.Y. Ying, Pressure-driven enzyme entrapment in siliceous mesocellular foam, Chem. Mater. 18 (2006) 643–649.
[35] Y.C. Lee, D. Yang, Determination of lysozyme activities in a microplate format, Anal. Biochem. 310 (2002) 223–224.
[36] T. Class, F.S. Ligler, Immobilized Biomolecules in Analysis: A Practical Approach, Oxford University Press, New York, 1998.
[37] H.H.P. Yiu, P.A. Wright, N.P. Botting, Enzyme immobilisation using SBA-15 mesoporous molecular sieves with functionalised surfaces, J. Mol. Catal. B: Enzyme 15 (2001) 81–92.
[38] K. Griebenow, A.M. Klibanov, On protein denaturation in aqueous-organic mixtures but not in pure organic solvents, J. Am. Chem. Soc. 118 (1996) 11695–11700.

[39] N. Brandes, P.B. Welzel, C. Werner, L.W. Kroh, Adsorption-induced conformational changes of proteins onto ceramic particles: Differential scanning calorimetry and FTIR analysis, J. Colloid Interface Sci. 299 (2006) 56–69.
[40] T.J. Su, J.R. Lu, R.K. Thomas, Z.F. Cui, J. Penfold, The effect of solution pH on the structure of Lysozyme layers adsorbed at the silica–water interface studied by neutron reflection, Langmuir 14 (1998) 438–445.
[41] R.C.F. Bonomo, L.A. Minim, J.S.R. Coimbra, R.C.I. Fontan, L.H. Mendes da Silva, V.P.R. Minim, Hydrophobic interaction adsorption of whey proteins: effect of temperature and salt concentration and thermodynamic analysis, J. Chromatogr. B 844 (2006) 6–14.
[42] T. Yamamoto, N. Fukui, A. Hori, Y. Matsui, Circular dichroism and fluorescence spectroscopy studies of the effect of cyclodextrins on the thermal stability of chicken egg white lysozyme in aqueous solution, J. Mol. Struct. 782 (2006) 60–66.
[43] C.A. Haynes, W. Norde, Structures and stabilities of adsorbed proteins, J. Colloid Interface Sci. 169 (1995) 313–328.
[44] B. Lee, F.M. Richards, The interpretation of protein structure: estimation of static accessibility, J. Mol. Biol. 55 (1971) 379–380.
[45] D.C. Phillips, The hen egg-white lysozyme molecule, Proc. Natl. Acad. Sci. 57 (1967) 484–495.
[46] L. Gao, Q. Gao, Q. Wang, S. Peng, J. Shi, Immobilization of hemoglobin at the galleries of layered niobate $HCa_2Nb_3O_{10}$, Biomaterials 26 (2005) 5267–5275.
[47] Y. Mei, L. Miller, W. Gao, R.A. Gross, Imaging the distribution and secondary structure of immobilized enzymes using infrared microspectroscopy, Biomacromolecules 4 (2003) 70–74.
[48] H. Larsericsdotter, S. Oscarsson, J. Buijs, Thermodynamic analysis of lysozyme adsorbed to silica, J. Colloid Interface Sci. 276 (2004) 261–268.
[49] M. Rankl, T. Ruckstuhl, M. Rabe, G.R.J. Artus, A. Walser, S. Seeger, Conformational reorientation of immunoglobulin G during nonspecific interaction with surfaces, ChemPhysChem 7 (2006) 837–846.
[50] D.J. States, M. Karplus, A model for electrostatic effects in proteins, J. Mol. Biol. 197 (1987) 122–130.